ELSEVIER

Chemical Engineering Journal 137 (2008) 282–293

Chemical Engineering Journal

www.elsevier.com/locate/cej

# On the estimation of the gas-side mass-transfer coefficient during the formation and ascension of bubbles

Ricardo C. Rodrigues, Cláudio P. Ribeiro Jr., Paulo L.C. Lage *

*Programa de Engenharia Química, COPPE, Universidade Federal do Rio de Janeiro, P.O. Box 68502, 21941-972 Rio de Janeiro, RJ, Brazil*

Received 26 August 2006; received in revised form 20 April 2007; accepted 24 April 2007

**Abstract**

Using a recently developed model for the simultaneous heat and multicomponent mass transfer during the formation and ascension of superheated bubbles, concentration profiles within a bubble during the stripping of diluted ethyl acetate solutions were determined and then used in the computation of the corresponding mass-transfer coefficient on the gas side, $k_G$. Both isothermal and non-isothermal bubbling cases were analysed. For the studied system, the importance of the gas-side resistance to mass transfer was clearly shown. During the formation stage, a large drop in $k_G$ with time was observed, as the mean gas velocity inside the bubble decreased on account of bubble growth. On the other hand, after bubble detachment, the value of $k_G$ remained approximately constant throughout the ascension time. For isothermal bubbling, it was demonstrated that the decomposition of the bubbling process into formation and ascension stages with two different constant mean $k_G$ values is a sound approach because their usage in a much simpler mass transfer model did not lead to significant errors in the prediction of the final ester concentration in the bubble. In the case of non-isothermal bubbling, an increase of almost 300 K in the gas inlet temperature had little effect on the $k_G$ values for both stages.


*Keywords:* Bubbles; Mass transfer; Bubble column; Gas stripping; Simultaneous heat and mass transfer; Bubble formation

## 1. Introduction

The contact of gases and liquids for mass-transfer purposes is a common operation in many industrial processes, such as gas absorption, humidification and gas stripping. Stirred vessels, packed towers, trickle bed reactors and bubble columns are devices extensively used in these applications. Bubble columns, in particular, exhibit many advantages over the other contactors, among which one can highlight the excellent mass-transfer properties, easy temperature control, capacity of operation with solids without erosion or plugging problems, decreased capital investment, lower operating and maintenance costs and greater simplicity of construction [1–4].

Most industrial applications of bubble columns involve the absorption of chemical species whose concentrations in the gas phase are high or whose solubilities in the liquid phase are low. In both cases, the main resistance to mass transfer lies in the liquid phase and, accordingly, the liquid-side mass-transfer coefficient, $k_L$, controls the mass-transfer resistance. Consequently, a vast amount of literature has been published on the estimation of $k_L$ during the ascension of bubbles in the last 40 years, including both empirical correlations [5–13] and mathematical models [14–16]. The bubble formation step has also been analysed, though to a lower extent [17–19].

Due to the aforementioned advantages, in the last two decades, additional applications using bubble columns have been investigated, including air stripping for the removal of ammonia from wastewater [20], removal of volatile organic compounds from water [21–23] and, more recently, gas stripping of aromas from fruit juices [24,25]. In these cases, on account of the dilution of the target components in the gas phase, the neglect of their diffusion within the bubble as a resistance to the overall mass-transfer process may lead to errors. Indeed, the importance of the gas-side resistance in gas stripping of diluted species has been highlighted by Pinheiro and Carvalho [26], Smith and Valsaraj [27] and Patoczka and Wilson [20]. For low-volatility compounds, Nirmalakhandan et al. [28] stated that the gas-phase mass-transfer coefficient, $k_G$, becomes more important than the one related to the liquid side. Nonetheless, only a few studies on the estimation of $k_G$ for bubbles have been conducted, the majority of which were restricted to the bubble ascension stage [20,29–31]. To the authors' knowledge, Rocha and Guedes de

* Corresponding author. Tel.: +55 21 2562 8346; fax: +55 21 2562 8300.
*E-mail address:* paulo@peq.coppe.ufrj.br (P.L.C. Lage).

1385-8947/$ – see front matter © 2007 Elsevier B.V. All rights reserved.
doi:10.1016/j.cej.2007.04.034

**Nomenclature**

| | |
|---|---|
| $A_b$ | bubble superficial area ($m^2$) |
| $c$ | mean concentration in the bubble ($kg/m^3$) |
| $Cp$ | heat capacity (J/kg K) |
| $d$ | diameter (m) |
| $D$ | diffusion coefficient (m/s) |
| $g$ | gravitational acceleration ($m/s^2$) |
| $G_I$ | gas injection flow rate ($m^3/s$) |
| $h$ | convective heat-transfer coefficient ($W/m^2$ K) |
| $H$ | height (m) |
| $\hat{H}$ | partial mass enthalpy (J/kg) |
| $k$ | convective mass-transfer coefficient (m/s) |
| $K$ | overall mass-transfer coefficient (m/s) |
| $\dot{m}^{ev}$ | vaporisation rate (kg/s) |
| $n$ | number of volatile species in the liquid phase |
| $N$ | mass-transfer flux ($kg/m^2$ s) |
| $P$ | pressure (Pa) |
| $r$ | radial coordinate (m) |
| $R_b$ | instantaneous bubble radius (m) |
| $\bar{R}_b$ | mean bubble radius (m) |
| $S$ | saturation |
| $t$ | time (s) |
| $T$ | temperature (K) |
| $t_{res}$ | bubble residence time (s) |
| $U$ | bubble ascension velocity (m/s) |
| $v$ | radial velocity inside the bubble (m/s) |
| $V_b$ | bubble volume ($m^3$) |
| $V_0$ | residual bubble volume at the orifice ($m^3$) |
| $Y$ | mass fraction |

*Greek letters*

| | |
|---|---|
| $\alpha$ | Henry's law constant |
| $\delta$ | volumetric Dirac delta function ($m^{-3}$) |
| $\lambda$ | thermal conductivity (W/m K) |
| $\nu$ | kinematic viscosity ($m^2/s$) |
| $\xi$ | constant defined by Eq. (5) |
| $\rho$ | density ($kg/m^3$) |
| $\sigma$ | surface tension (N/m) |
| $\tau$ | dimensionless time, $t/t_{res}$ |

*Subscripts*

| | |
|---|---|
| a | ascension stage |
| b | bubble |
| bb | bubbling |
| eq | equivalent |
| f | at the end of bubble formation |
| G | gas phase |
| $i$ | component $i$ |
| I | injection condition |
| L | liquid phase |
| $n+1$ | injected gas |
| o | orifice |
| res | at the end of bubble residence time |

*Superscripts*

| | |
|---|---|
| o | pure component |
| s | bubble surface |
| sat | saturation |
| 0 | value at $t = 0$ |
| $\infty$ | bulk region |

Carvalho [18] and Carvalho et al. [32] have been the only ones to report gas-phase volumetric mass transfer coefficients related to bubble formation. These works suggested that the mass transfer during bubbling should be modelled by splitting it into two stages: formation and ascension of bubbles.

In this work, the matter of gas-side mass-transfer resistance during the stripping of volatile aroma compounds from diluted aqueous solutions was addressed. With the aid of the model recently developed by Ribeiro et al. [33] for the simultaneous heat and multicomponent mass transfer during the formation and ascension of superheated bubbles, concentration profiles of the volatile aroma compound within the bubble were determined and then used in the computation of the instantaneous $k_G$ value throughout the bubble residence time. Both isothermal and non isothermal bubbling cases were analysed and ethyl acetate was chosen as the model aroma compound. Moreover, different mean values of $k_G$ were determined for each stage and their adequacy in representing the mass-transfer as a two-stage process was assessed by using a much simpler mass-transfer model.

## 2. Mathematical formulation

Most mass-transfer processes involve the contact of two or more phases and the transfer of solutes across a phase boundary. In gas stripping, for example, a solute diffuses through the carrier liquid phase to a gas surface, where it dissolves and is transferred by diffusion and/or convective mixing into the gas phase. Several mathematical models have been formulated to describe the transfer across a phase boundary. The two-resistance theory, developed by Lewis and Whitman [34], assumes that the resistances to mass transfer are confined to two thin stagnant films on both sides of the gas–liquid interface. The interface itself does not offer any resistance to solute transfer and the interfacial concentrations are, therefore, in local equilibrium and can be calculated using thermodynamic relations. The reliability of this theory has been the subject of a great amount of study and, according to Treybal [35], a review of the obtained results indicates that the departure from equilibrium at the interface must be a rarity.

Using the two-resistance theory, the mass-transfer flux $N$ ($kg/m^2$ s) across the interface under steady-state conditions is given by

$$N = K\left(c_L^{\infty} - \frac{c_G}{\alpha}\right) \quad (1)$$

in which $\alpha$ is the Henry's law constant, $c_L^{\infty}$ ($kg/m^3$) is the solute concentration in the bulk liquid phase, $c_G$ ($kg/m^3$) is the mean concentration of solute in the gas phase and $K$ (m/s) is the

so-called overall mass-transfer coefficient, whose value is determined using the gas and liquid-side mass-transfer coefficients:

$$\frac{1}{K} = \frac{1}{k_L} + \frac{1}{\alpha k_G} \tag{2}$$

During the stripping of a volatile compound without any chemical reaction in the gas phase, the material balance on either a forming or ascending bubble enables one to write the following relation:

$$\frac{d}{dt}(c_G V_b) - K A_b \left(c_L^\infty - \frac{c_G}{\alpha}\right) = 0 \tag{3}$$

in which $V_b$ ($m^3$) and $A_b$ ($m^2$) are, respectively, the bubble volume and superficial area and $t$ (s) is time.

For an isothermal process, provided that the flux of the target component and the hydrostatic pressure head are small, bubble volume variation may be neglected in the ascension stage. In addition, if the value of $K$ is constant, Eq. (3) can be integrated to give the variation of solute concentration in the bubble with time:

$$\frac{c_G(t) - \alpha c_L^\infty}{c_G^0 - \alpha c_L^\infty} = e^{-\xi t} \tag{4}$$

$$\xi \equiv \frac{3K}{\alpha R_b} \tag{5}$$

being $R_b$ (m) the bubble radius and $c_G^0$ ($kg/m^3$) the mean solute concentration in the bubble for $t = 0$.

On the other hand, for the formation stage, bubble volume variation has to be taken into account. Considering isothermal bubble formation in the constant-flow-rate regime [36], the bubble volume as a function of time is given by

$$V_b(t) = V_0 + G_I t \tag{6}$$

where $V_0$ ($m^3$) is the residual bubble volume attached to the orifice at $t = 0$ and $G_I$ ($m^3/s$) is the gas injection flow rate. In Eq. (6), the mass flux of the target component is assumed to be small enough to justify the neglect of its effect upon the bubble volume.

Utilising Eq. (6), one can rewrite Eq. (3) in order to obtain the following non-linear ordinary differential equation:

$$\frac{dc_G}{dt} + \frac{c_G}{(V_0/G_I) + t} + \xi(c_G - \alpha c_L^\infty) = 0 \tag{7}$$

For a given set of $K$, $c_L^\infty$ and $G_I$ values, Eq. (7) can be solved numerically to give the transient evolution of the mean solute concentration in the bubble during the formation stage.

### 2.1. Liquid-side mass-transfer coefficient

As a result of the widespread use of bubble columns in the chemical and biochemical process industries and the importance of the liquid-side mass-transfer coefficient as a design parameter for these units, a great number of empirical correlations can be found in the literature for predicting the $k_L$ value for bubbling processes [1]. After reviewing the available literature, both Shah et al. [2] and Deckwer and Schumpe [4] recommended the use of the following equation, originally proposed by Akita and Yoshida [7] based on their data for different gas–liquid systems:

$$k_{L,i} = 0.25 \frac{D_{i,L}}{R_b} \left(\frac{\nu_L}{D_{i,L}}\right)^{1/2} \left(\frac{8 g R_b^3}{\nu_L^2}\right)^{1/4} \left(\frac{4 g R_b^2 \rho_L}{\sigma}\right)^{3/8} \tag{8}$$

In this work, in order to investigate the influence of the adopted $k_L$ correlation upon the obtained results, apart from Eq. (7), three other relations were also tested, namely the ones proposed by Calderbank and Moo-Young [5] for large bubbles, Hikita et al. [9] and Öztürk et al. [11]. In the development of these correlations, no distinction between the individual contributions of the formation and ascension steps was made. Therefore, the same $k_L$ value was utilised for both bubbling steps. Its value was computed using the mean bubble radius predicted by the model of Ribeiro et al. [33]:

$$\bar{R}_b = \frac{\int_0^t R_b(t')\,dt'}{t} \tag{9}$$

Even though there exists a model for $k_L$ prediction during the formation step, namely the one developed by Walia and Vir [17], it was not regarded as suitable because it was developed for drops with the assumption of density ratios close to 1, which clearly does not hold for bubbles.

### 2.2. Gas-side mass-transfer coefficient

A detailed model for coupled heat and multicomponent mass transfer in bubbles, namely the one developed by Ribeiro et al. [33], was adopted for computing the values of $k_G$. According to this model, the bubble is spherical throughout its residence time in the liquid and the diffusive fluxes are appropriately described by Fick's law. In the formation stage, gas injection is modelled as a point source located at the bubble centre which emits gas at the inlet conditions. Gas property variations, as well as bubble radius changes, are taken into account. For a liquid phase containing $n$ volatile species, this model comprises the following simplified forms of the continuity, species and energy conservation equations for the bubble:

$$\frac{\partial \rho_G}{\partial t} + \frac{1}{r^2}\frac{\partial}{\partial r}(r^2 \rho_G v) = \rho_I G_I \delta(r) \tag{10}$$

$$\frac{\partial}{\partial t}(\rho_G Y_i) + \frac{1}{r^2}\frac{\partial}{\partial r}\left[r^2 \rho_G \left(Y_i v - D_i \frac{\partial Y_i}{\partial r}\right)\right] = \rho_I G_I Y_{i,I} \delta(r), \quad i = 1, 2, \ldots, n \tag{11}$$

$$\frac{\partial}{\partial t}(\rho_G C p_G T) + \frac{1}{r^2}\frac{\partial}{\partial r}(r^2 \rho_G v C p_G T) - \frac{1}{r^2}\frac{\partial}{\partial r}\left(r^2 \lambda_G \frac{\partial T}{\partial r}\right) = \rho_I G_I \delta(r) \sum_{i=1}^{n+1} Y_{i,I} \overline{C_i^0 p} T_I + \sum_{i=1}^{n} (\overline{C_i^0 p} - \overline{C_{n+1}^0 p}) \frac{\partial}{\partial r} \times \left(r^2 T \rho_G D_i \frac{\partial Y_i}{\partial r}\right) \tag{12}$$

in which the index $n + 1$ refers to the injected gas, assumed to be insoluble in the liquid.

Eqs. (10)–(12) are valid for the formation stage; the corresponding equations for the ascension stage are obtained by setting $G_I = 0$. In both cases, the relations are subjected to the following boundary conditions:

$$-\frac{\sum_{i=1}^{n} \dot{m}_i^{ev}}{4\pi R_b^2} = \rho_G^s \left( v^s - \frac{dR_b}{dt} \right) \quad \text{at} \quad r = R_b(t) \tag{13}$$

$$\rho_G D_i \left. \frac{\partial Y_i}{\partial r} \right|_{r=R_b(t)} = \frac{1}{4\pi R_b^2} \left( \dot{m}_i^{ev} - Y_i^s \sum_{i=1}^{n} \dot{m}_i^{ev} \right) \quad \text{at} \quad r = R_b(t) \tag{14}$$

$$-\lambda_G \left. \frac{\partial T}{\partial r} \right|_{r=R_b(t)} = h_L(T^s - T_L^\infty) + \frac{\sum_{i=1}^{n} \dot{m}_i^{ev} [\hat{H}_{i,G}(T^s) - \hat{H}_{i,L}(T^s)]}{4\pi R_b^2}$$

$$\text{at} \quad r = R_b(t) \tag{15}$$

In order to predict bubble detachment from the orifice and its ascension, Eqs. (10)–(12) have to be solved together with a corresponding bubble dynamics model. As detailed by Ribeiro et al. [33], for the formation stage, a slight modification of the model proposed by Davidson and Schuler [37] was utilised, whilst, for the ascension stage, a force balance was written, taking into account inertial, added mass, buoyancy and drag effects.

The simultaneous solution of Eqs. (10)–(12) gives the radial concentration profiles in the bubble for each volatile species at each time $t$ up to its residence time, $t_{res}$. Therefore, the mean solute concentration in the bubble may be computed as follows:

$$c_{i,G}(t) = 3[R_b(t)]^{-3} \int_0^{R_b(t)} \rho_G(r,t) Y_i(r,t) r^2 \, dr \tag{16}$$

Furthermore, the vaporisation rate of each component, the bubble radius, the liquid-phase concentration of component $i$ at bubble surface, $c_{L,i}^s$, and the Henry's law constant are also known from the solution of Eqs. (10)–(12). Thus, from the definition of the gas-side mass-transfer coefficient, it follows that:

$$k_{G,i}(t) = \frac{\dot{m}_i^{ev}(t)}{4\pi[R_b(t)]^2[\alpha_i(t) c_{L,i}^s(t) - c_{G,i}(t)]} \tag{17}$$

The $c_{L,i}^s$ value is related to $c_L^\infty$ by the flux relation:

$$\dot{m}_i^{ev} = 4\pi R_b^2 k_{L,i}(c_{L,i}^\infty - c_{L,i}^s) \tag{18}$$

In order to test the model with a constant overall resistance, average $k_G$ values are required. In this work, three different $k_G$ averages were investigated: (i) simple time-averaged $k_G$, Eq. (19); (ii) time-averaged $k_G$ weighted by area, Eq. (20); (iii) time-averaged $k_G$ weighted by the component $i$ flux, Eq. (21).

$$\bar{k}_G^1 = \frac{\int_0^t k_G(t')\,dt'}{t} \tag{19}$$

$$\bar{k}_G^2 = \frac{\int_0^t k_G(t') A(t')\,dt'}{\int_0^t A(t')\,dt'} \tag{20}$$

$$\bar{k}_G^3 = \frac{\int_0^t k_G(t') A(t') [c_{G,i}^s(t') - c_G(t')]\,dt'}{\int_0^t A(t') [c_{G,i}^s(t') - c_G(t')]\,dt'} \tag{21}$$

## 3. Numerical procedure

As detailed by Ribeiro et al. [33], the model for coupled heat and mass transfer in bubbles was written in a dimensionless form and then solved by the method of lines using finite-volume spatial discretisation. The system of non-linear differential equations obtained after discretisation was solved together with the appropriate dynamics model utilising the DASSL routine [38], whose absolute and relative tolerances were set to $10^{-10}$ and $10^{-8}$, respectively.

In the case of isothermal bubbling, for both the bubble formation and ascension stages, time-averaged $k_G$ values were computed by trapezoidal integration along the corresponding time interval following Eqs. (19)–(21). These values were substituted into Eq. (2) for calculating the respective overall mass-transfer coefficients. Once these values were known, the models given by Eq. (4) and Eqs. (5) and (7) could be tested for the ascension and formation stages, respectively, being the latter solved by the DIVPRK routine of the IMSL library, which couples the Runge-Kutta-Verner fifth-order and sixth-order methods.

All simulations were performed for the air–water–ethyl acetate system. All physical properties of the pure substances were evaluated using the correlations presented by Daubert and Danner [39]. Water-air binary diffusion coefficients as a function of temperature were calculated using the relation developed by Lage [40], whereas the values for the ethyl acetate–air system were estimated by the correlation of Fuller et al. (Reid et al. [41]). The ideal gas law was employed for calculating the gas mixture density, and the mixture thermal conductivity was estimated by the Mason and Saxena's modification of the Wassiljewa's equation [41]. The gas mixture specific heat was computed based upon the ideal solution behaviour. For each component, the mean specific heat was obtained from its definition, using the inlet gas and liquid temperatures as the integration limits. The Henry's law constants for ethyl acetate as a function of temperature were evaluated based upon the corresponding infinite dilution activity coefficients reported by Sancho et al. [42].

## 4. Results and discussion

### 4.1. Isothermal bubbling

Initially, the isothermal air stripping of a diluted ethyl acetate solution at four different operating temperatures was considered. The conditions adopted to perform the simulations are detailed in Table 1. These conditions were established based on the experimental runs carried out by Ribeiro et al. [24] for this system. All simulations were performed considering the inlet air saturated with water vapour at the operating temperature as an initial

Table 1
Simulation conditions adopted for the isothermal air stripping of a diluted ethyl acetate solution at four different temperatures (298, 318, 333 and 353 K)

| | |
|---|---|
| Aroma concentration in the liquid, $c_L^{\infty}$ (kg/m$^3$) | 1.00 |
| Orifice diameter in the sparger, $d_o$ (mm) | 0.50 |
| Gas injection flow rate in the orifice, $G_I$ (mg/s) | 0.4507 |
| Pressure, $P$ (kPa) | 101.32 |
| Bubbling height, $H_b$ (mm) | 63.3 |

condition. The simulation results for the mean concentration of ethyl acetate in the bubble and the gas-side mass-transfer coefficient are plotted in Fig. 1(a) as a function of the dimensionless time, $\tau$, defined as the ratio $t/t_{res}$.

Regardless of the liquid temperature, due to the mass transfer brought about by the concentration gradients between the liquid and the gas phases, the aroma concentration in the bubble increases progressively as the bubble moves through the liquid, reaching its saturation value close to the end of the ascension stage. However, a clear distinction between the rates of concentration increase related to the formation and ascension stages can be perceived, there existing a clear cusp in the concentration profile at the moment of bubble detachment. As the concentration approaches saturation, the driving force for mass transfer is reduced. Thus, the aroma mass flux into the bubble decreases and, accordingly, the rate of concentration increase falls. Even

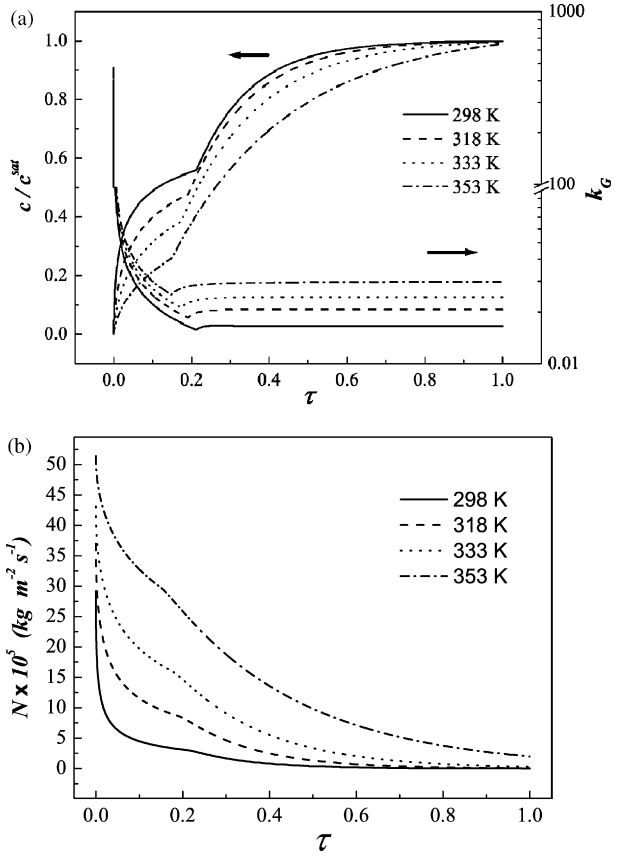


Fig. 1. Simulation results for the isothermal air stripping of a diluted ethyl acetate solution at different operating temperatures: (a) mean aroma concentration in the bubble and gas-side mass-transfer coefficient and (b) aroma flux into the bubble.

though this reasoning elucidates the individual shapes of the concentration profile in Fig. 1(a) for each stage of the bubble residence time, it does not explain the existence of the cusp, which could be related to an augmentation of the aroma flux into the bubble after the formation stage. However, as evidenced in Fig. 1(b), the aroma flux falls progressively from the formation to the ascension stage as the concentration inside the bubble increases, which is consistent with the reduction in the driving force for mass transfer. The cusp actually appears due to the interruption of gas injection into the bubble at the moment of detachment. Throughout the formation stage, aroma vaporisation into the bubble takes place in tandem with gas injection, so that the increase in the aroma amount inside the bubble is partially counterbalanced by the augmentation of the mass of inert gas, resulting in a lower net increase in the aroma concentration. At the moment of detachment, gas injection into the bubble is interrupted, and, accordingly, the previous partial counterbalance for the aroma flux into the bubble is eliminated, leading to a significant change in the concentration increasing rate, which results in the cusp in the concentration profiles shown in Fig. 1(a).

A comparison between the individual profiles in Fig. 1(a) shows that, the higher the liquid temperature, the lower the saturation degree of the bubble for a given time. This stems from the significant increase in the saturation concentration of the ester in the bubble with the liquid temperature, brought about by the effect of the later on the saturation pressure of the ester and its activity coefficient. As evidenced in Fig. 1(b), the mass flux of ester into the bubble grows significantly with the liquid temperature, a fact that is basically related to the augmentation of the Henry's law constant with $T_L$, which, for a given ester concentration in the liquid phase, ensures a higher driving force for mass transfer, as evidenced in Eq. (1). Consequently, for a given set of operating conditions, the higher the liquid temperature, the larger the amount of ester stripped from the liquid.

With regard to the gas-side mass-transfer coefficient, whichever the operating temperature, the results in Fig. 1(a) indicate a sheer drop in this parameter at the very beginning of the formation stage. As bubble formation proceeds, this drop becomes less significant but is still considerable. In total, the $k_G$ values for the formation stage cover almost four orders of magnitude. On the other hand, as far as the ascension stage is concerned, the changes in $k_G$, though still present, are much less pronounced.

The model of Ribeiro et al. [33], employed in this work, considers both the diffusive and the convective contributions to the radial mass flux in the bubble (see Eq. (11)). The variation in $k_G$ with the residence time is closely related to the changes in the convective contribution, which can be analysed based upon the radial velocity profiles in the bubble, whose evolution with the dimensionless residence time for $T_L = 298$ K is portrayed in Fig. 2. At the very beginning of bubble formation, the injection flow rate is distributed within a small bubble volume, resulting in high radial velocities, which guarantee high convective fluxes, and, accordingly, high values of $k_G$ are verified. As the bubble grows and since $G_I$ is kept constant throughout the formation stage, the gas radial velocity has to fall, reducing the convec-

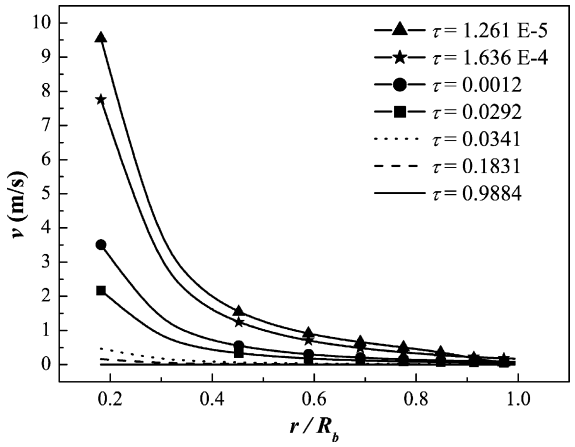


Fig. 2. Radial velocity profiles for different bubble residence times during the isothermal air-stripping of a dilute ethyl acetate solution at 298 K.

tive contribution to the mass flux and, consequently, the value of $k_G$. For a constant gas injection rate, the smaller the bubble, the greater the effect of bubble growth upon the radial velocity, which accounts for the sheer drops in it, and, consequently, in $k_G$, observed at the very beginning of the formation stage. After detachment, as the gas injection into the bubble ceases, radial velocities can only arise from bubble volume changes brought about by either temperature variation or vaporisation fluxes. Since the analysed case is isothermal and the flux of the target component is not high enough to increase the bubble volume significantly, the radial velocity throughout the ascension stage remains approximately constant and quite close to 0, so that no significant variation in $k_G$ is observed.

As the liquid temperature is raised, an increase in $k_G$ is noticed in Fig. 1(a) but for the very beginning of the formation stage. This effect can be reasoned in terms of two different contributions, depending on the bubbling stage. In the case of bubble formation, since isothermal bubbling is considered and the mass flow rate of the inlet gas was kept constant, a higher temperature implies a higher gas volumetric flow rate in the orifice, which enhances convection inside the bubble and then increases $k_G$. This effect is not significant at the very beginning due to the high radial velocities inside the growing bubble (see Fig. 2), but becomes progressively more important as formation proceeds. As far as the ascension stage is concerned, such reasoning does not apply, as gas injection is interrupted. What occurs in this case is mainly a consequence of the increase in the diffusion coefficient inside the bubble with the operating temperature.

Another interesting aspect of Fig. 1(a) to which attention should be drawn is the fact that, for the studied cases, even though the formation stage corresponds only to about 20% at 298 K and 15% at 353 K of the total bubble residence time, the aroma saturation degrees reached in this stage were between 56% at 298 K and 20% at 353 K, clearly evidencing the importance of the formation stage to the mass-transfer process during gas sparging through liquids. This result is in perfect agreement with the observations of Carvalho et al. [32], who have reported the formation stage to be particularly effective in those mass-transfer processes in which the gas-side resistance plays an important role.

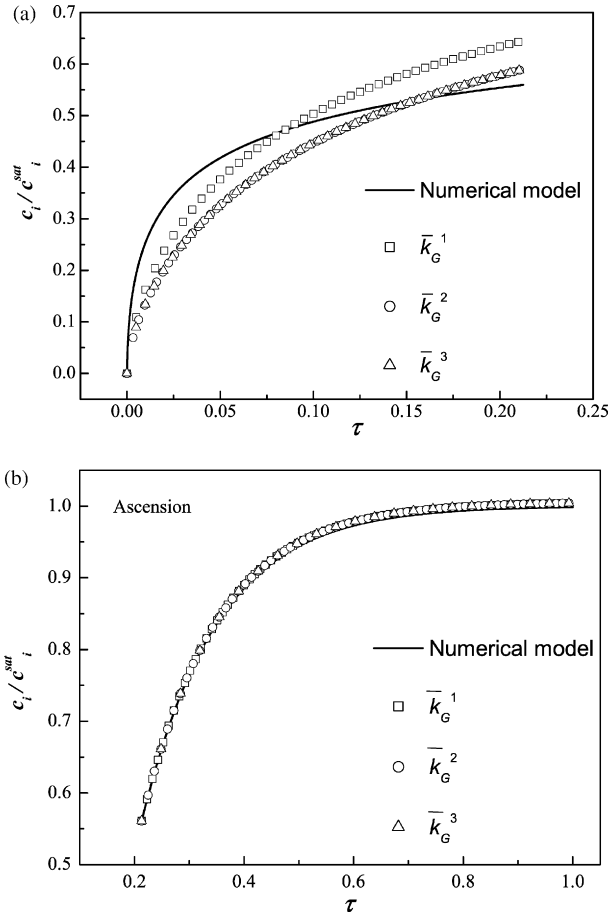


Fig. 3. Comparison between ester concentrations in the bubble predicted by the numerical model of Ribeiro et al. [33] and the constant-K model using different $k_G$ averages for the formation (a) and ascension (b) stages at 298 K.

In most practical applications, it is common to admit a constant overall resistance to mass transfer expressed in terms of a mean $K$ value, calculated based upon mean values of $k_L$ and $k_G$ for the whole bubble residence time. Therefore, it is important to evaluate whether the previous results for the evolution of the mean concentration of ethyl acetate in the bubble can be reproduced using time-averaged $k_G$ values for each bubbling stage. Following the procedure previously described in Section 3, the $k_G$ data in Fig. 1(a) were utilised in the calculation of the corresponding time-averaged values for both the formation and the ascension stages, which, together with the $k_L$ value, were used for computing the mean $K$ value in each bubbling step. Once the $K$ values were known, Eqs. (4), (5) and (7) were respectively used for the ascension and formation stages.

Fig. 3 shows the results of mean ester concentration in the bubble at 298 K using the three different $k_G$ averages given by Eqs. (19)–(21). As regards the formation stage, it can be seen that none of them were able to represent the transient evolution of the ethyl acetate concentration given by the detailed numerical model of Ribeiro et al. [33], a fact that is linked to the considerable variation of $k_G$ with time during bubble formation (Fig. 1(a)). The simple time-averaged $k_G$, $\bar{k}_G^1$, presented the worst result, with a deviation of 15% in the concentration value at the end of the bubble formation. The averages given by Eqs.

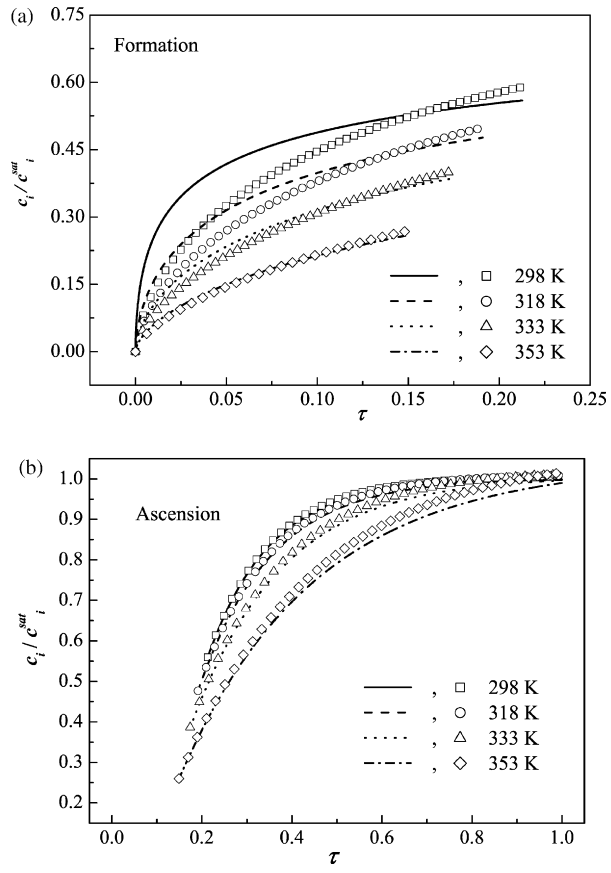


Fig. 4. Comparison between the transient behaviours of aroma concentration in the bubble at different temperatures predicted by the numerical model of Ribeiro et al. [33](lines) and by the constant-K model (symbols) for both stages: (a) formation and (b) ascension.

(20) and (21) gave similar results. Though unable to capture the transient behaviour of the system, these averages did enable the estimation of a saturation degree at the moment of detachment that is close to the one given by the numerical model, with deviations around 5%.

On the other hand, for the ascension stage, as the changes in the gas-side mass-transfer coefficient were much less pronounced, the transient evolution of the ester concentration in the bubble was properly reproduced regardless of the $k_G$ average adopted, leading to deviations lower than 1% between the concentration values obtained by the constant-K and numerical models at the end of the bubble ascension at 298 K. Based on these results and considering that $\bar{k}_G^2$ is simpler to compute than $\bar{k}_G^3$, the former was chosen as the standard average to perform all further calculations in this work.

The concentration values computed with the constant-K model for all operating temperatures analysed in this work are compared in Fig. 4 with the corresponding values given by the numerical model of Ribeiro et al. [33]. It is clear in this figure that the use of $\bar{k}_G^2$ enables a good estimation of the final ester concentration in the bubble with the constant-K model for either the formation or ascension steps within the operating range considered. As shown in Fig. 4(b), for bubble ascension, even the transient behaviour can be well described by the constant-K model. During bubble formation, this is only true for $T > 333$ K and the deviations increase as the temperature is reduced.

As the constant-K model represents this mass-transfer problem reasonably well, it can be employed to demonstrate the importance of the gas-side resistance to mass transfer in the analysed problem. Thus, for the ascension stage, keeping all other parameters constant, the overall mass-transfer coefficient $K$ was calculated neglecting the gas-side contribution, that is, by letting $k_G \to \infty$. The results obtained for the mean aroma concentration in the bubble at different operating conditions are compared with the ones associated with the model of Ribeiro et al. [33] in Fig. 5. As evidenced in the aforementioned figure, for the analysed case, the neglect of the gas-side resistance during bubble ascension is rather inappropriate, leading to an overestimation of the ethyl acetate flux, and, consequently, of the aroma concentration in the bubble. The lower the operating temperature, the more pronounced the error caused by the neglect of $k_G$. As an example, when this simplification is applied for $T$ =298 K, an aroma saturation degree of 98% is obtained before half the bubble residence time has elapsed ($\tau = 0.405$), whereas, according to the model of Ribeiro et al. [33], such a saturation degree can only be achieved after 71% of the residence time.

The reason for the disagreement verified in Fig. 5 becomes clearer by means of an analysis of the individual contributions of the gas- and liquid-side resistances to the calculation of $K$, which are plotted in Fig. 6 as a function of the dimensionless residence time for both the formation and ascension stages.

First of all, it is evident from Fig. 6 that, but for the very beginning of the formation stage, one cannot regard the mass-transfer process as one-phase controlled within the adopted operating range. In particular, for the ascension stage, one phase always contributes with at least 20% of the total resistance, which explains the deviations previously observed in Fig. 5. In the case of the two smallest temperatures, a striking aspect of the analysed process is revealed, namely, an inversion of the main contributor to the overall mass-transfer resistance during the bubble residence time. At the beginning of bubble formation, on account of the high radial velocities inside the bubble and the resulting high convective fluxes, most of the mass-transfer resistance lies within the liquid phase. As the bubble grows, the radial velocities inside it decrease, causing a reduction in the $k_G$ value, so that the gas-side contribution to the overall resistance increases. Eventually, a point is reached during the formation stage at which the individual contributions of the two phases become equal. From this point on, as the bubble keeps growing and $k_G$ falls accordingly, the gas-side resistance surpasses the liquid-side one. At the moment of detachment, the gas-side contribution at 298 K accounts for about 76% of the overall resistance. During the ascension stage, as $k_G$ remains approximately constant (Fig. 1), the contributions from each phase do not vary significantly. As the operating temperature is raised, the saturation pressure and the activity coefficient of the ester in the liquid phase grow considerably, leading to an increase in the Henry's law constant $\alpha$ and, consequently, to a decrease in the resistance to mass transfer on the gas side. As a result, the importance of the gas-side contribution falls as the temperature increases, which explains the lower discrepancies verified in Fig. 5 for higher tem-

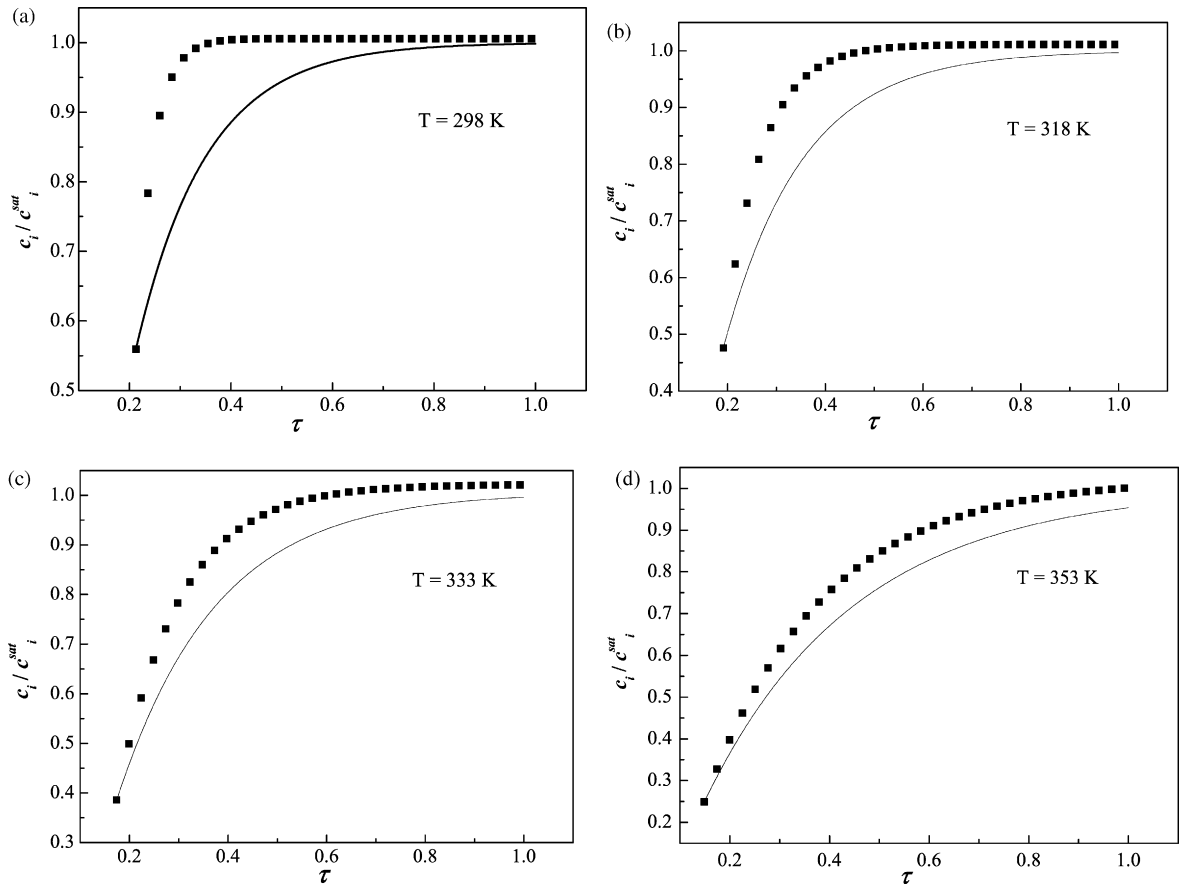


Fig. 5. Transient evolution of the mean ester concentration in the bubble during the ascension stage at different temperatures computed with (lines) and without (symbols) the gas-side mass-transfer resistance: (a) 298 K, (b) 318 K, (c) 333 K and (d) 353 K.

peratures. Moreover, for $T = 333$ K, this significant increase in $\alpha$ already turns the gas-side contribution small enough to eliminate the inversion of the main mass-transfer resistance during the bubble residence time previously verified at 298 and 318 K.

Considering the vast amount of correlations available in the literature for estimating $k_L$ and the considerable discrepancy exhibited between some of them, one could wonder if this importance of the gas-side mass-transfer resistance is a general outcome or only a correlation-related effect. Therefore, an analysis of the sensitivity of the model results to the employed $k_L$ correlation was conducted. This analysis was carried out for $T = 298$ K since, at this operating temperature, the gas-side resistance was the greatest. Apart from the Akita and Yoshida [7] correlation, utilised to obtain all results presented so far, three other correlations were tested [5,9,11]. The simulation results for the gas-side contribution to the overall mass-transfer resistance considering these four correlations are compared in Fig. 7.

Table 2 shows the $k_L$ values estimated with different correlations. As expected, regardless of the operating temperature, significant differences between them are observed. These differences are reflected in the nominal values of the gas and liquid contributions to the overall mass-transfer resistance, as evidenced in Fig. 7 for $T = 298$ K. However, it is clear in this figure that the gas-side mass-transfer resistance is indeed rather important in the process, whichever the correlation employed for $k_L$.

#### 4.1.1. The equivalent height of bubbling

Rocha and Guedes de Carvalho [18] defined the height equivalent to the inlet port as the height of the gas-liquid column that would give a fractional amount of mass transfer equal to that observed at the nozzle outlet, that is, the bubble formation zone. They used nozzles with diameters of 5 and 10 mm for the absorption of mixtures of $NH_3$ in HCl solution, a system in which the gas-phase resistance is basically the only existing mass-transfer resistance. They calculated the equivalent height of bubbling, $H_{eq}$, to be 6–13 cm for different nozzle flow rates and two different absorbers. For $O_2$ physical absorption in water, in which the liquid-phase resistance is dominant, they estimated $H_{eq}$ to be between 2 and 4 cm. In another experimental study, Guedes de Carvalho et al. [32] reported experiments using the

Table 2
Liquid-side mass-transfer coefficient values estimated with different correlations with $\bar{R}_b = 1.94$ mm

| | Temperature (K) | | | |
|---|---|---|---|---|
| | 298 | 318 | 333 | 353 |
| Correlations | $k_L$ ($\times 10^4$ m/s) | | | |
| Calderbank and Moo-Young [5] | 1.75 | 2.69 | 3.54 | 4.82 |
| Akita and Yoshida [7] | 2.94 | 3.73 | 4.36 | 5.26 |
| Hikita et al. [9] | 3.05 | 4.06 | 4.87 | 6.04 |
| Öztürk et al. [11] | 4.47 | 5.37 | 5.98 | 6.71 |

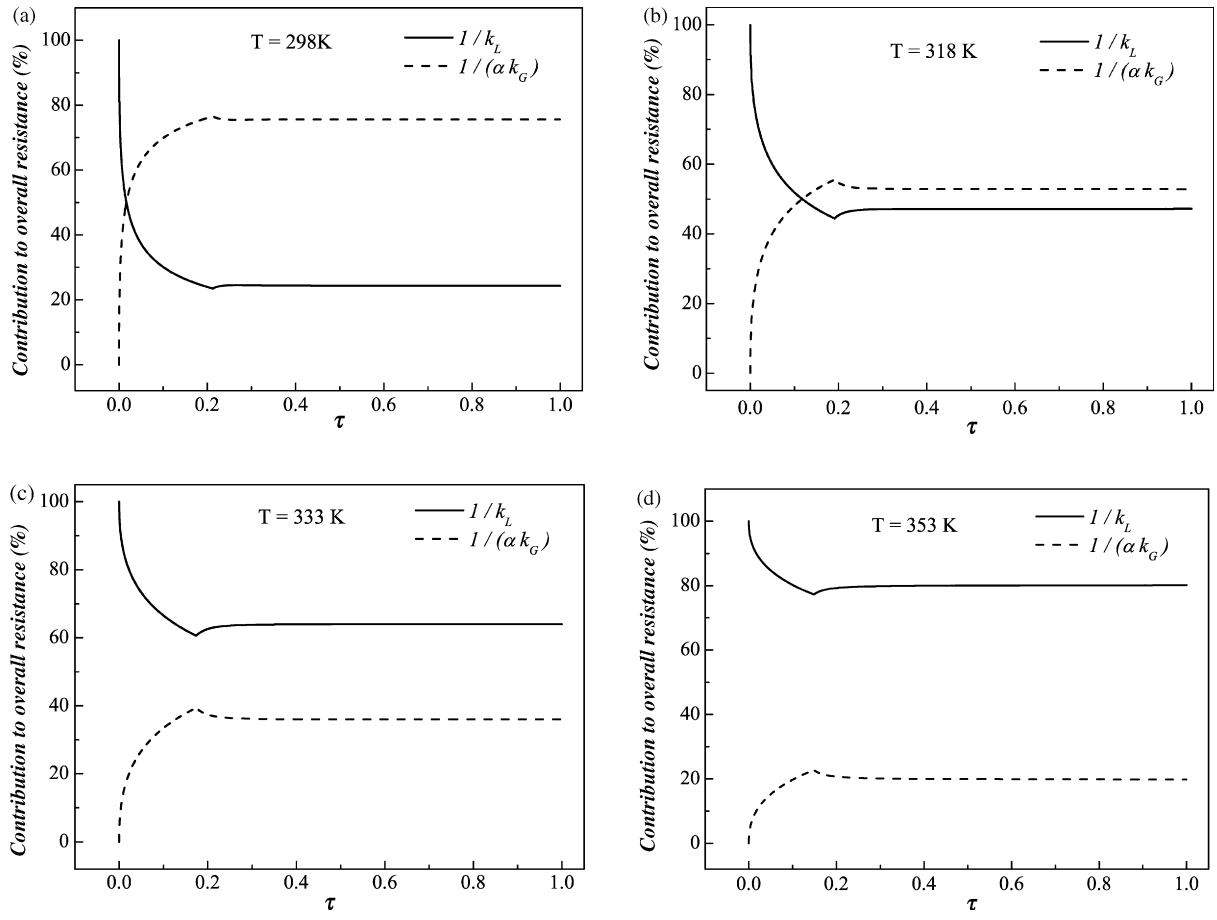


Fig. 6. Individual contributions of liquid- and gas-side terms to the overall mass-transfer resistance during the isothermal air-stripping of a diluted ethyl acetate solution at different liquid temperatures.

same gas–liquid systems in absorbers with nozzles whose diameters were 2 and 3 mm. They also calculated the $H_{eq}$ for the cases where either the gas-phase resistance or the liquid-phase resistance dominates, obtaining values in the 10–20 cm range.

Although the detailed heat and mass transfer model given by Ribeiro et al. [33] cannot be easily adapted to the reactive $NH_3$–HCl system, it is interesting to calculate the equivalent height of bubbling from its predictions for the air-ethyl acetate–water system. Following the definition given by Rocha and Guedes de Carvalho [18], the saturation at the end of the formation stage, $S = c_{G,f}/\alpha c_L^{\infty} = c_{G,f}/c_G^{sat}$, calculated from the detailed model, is used in the simplified model for bubble ascension, Eq. (4), together with $c_G^0 = 0$, to give $S = 1 - e^{\xi t_a}$. The ascension time, $t_a$, thus determined, was multiplied by the bubble ascension velocity, $U$, calculated by the detailed model, to give the equivalent height of bubbling for the present gas–liquid system. For the four isothermal simulations shown in Fig. 1, $H_{eq}$ values varied from 0.9 to 0.6 cm, decreasing as the operation temperature was raised.

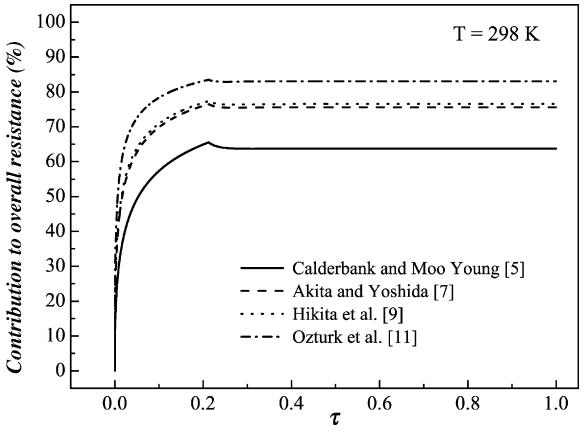


Fig. 7. Comparison of the gas-side contributions to the overall mass-transfer resistance computed using different correlations for estimating $k_L$ in the isothermal stripping of a dilute ethyl acetate solution at 298 K.

These values are quite different from those obtained by Rocha and Guedes de Carvalho [18] and Guedes de Carvalho et al. [32]. The main reason is the large dependence of $H_{eq}$ on the bubble diameter. For large bubbles, this dependence can be easily derived by assuming that $U \propto d_b^{1/2}$ and noting that, for a fixed $S$, $\xi t_a$ = constant or $t_a \propto d_b$. Therefore, $H_{eq} = t_a U \propto d_b^{3/2}$. Although not explicitly given, the bubble diameters in the work of Rocha and Guedes de Carvalho [18] can be inferred from their Fig. 13 to be in the 2–4 cm range. This size range may explain the more than two-fold variation of $H_{eq}$ values they obtained for the $NH_3$–HCl system. It also explains the large discrepancy between our $H_{eq}$ values for the air-ethyl acetate–water system

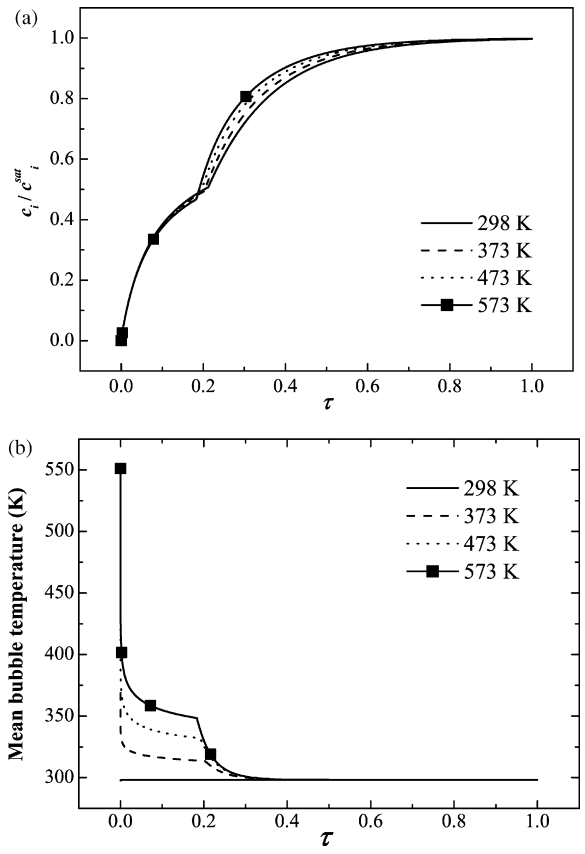


Fig. 8. Simulation results for the air stripping of a diluted ethyl acetate solution using various gas inlet temperatures: (a) mean aroma concentration in the bubble; (b) mean bubble temperature.

and the values given in [18,32]. If the $d_b^{3/2}$ dependence were valid down to our bubble size ($d_b \cong 0.4$ cm), it would predict $H_{eq}$ values around 7–10 cm for a bubble of 2 cm in diameter, which agrees with the range of $H_{eq}$ obtained in [18,32]. Unfortunately, no $d_b$ data were given by Guedes de Carvalho et al. [32].

Though interesting to show the relative importance of the bubble formation on the mass transfer for a given process, it is clear that $H_{eq}$ data cannot be compared among different processes of gas–liquid systems if the bubble diameter is not known.

### 4.2. Non-isothermal bubbling

In view of the fact that the model of Ribeiro et al. [33] considers coupled heat and multicomponent mass transfer in bubbles, non-isothermal air stripping of aromas could also be analysed. Keeping the mass flow rate of injected gas constant, as well as the liquid temperature (298 K), simulations were performed for three different gas inlet temperatures, using the correlation of Akita and Yoshida [7] for estimating $k_L$. The results for the mean aroma concentration and the mean temperature in the bubble as a function of the dimensionless time are presented in Fig. 8.

An analysis of the results in Fig. 8(a) reveals that, as far as the formation stage is concerned, there is little difference between the aroma saturation in the bubble obtained for the different gas inlet temperatures, even though a temperature variation of almost 300 K was considered. Nevertheless, during the ascension stage, the higher the gas inlet temperature, the faster the rate of increase in the mean aroma saturation in the bubble. As regards the bubble mean temperature, the data in Fig. 8(b) indicate a fast drop in the value of this parameter during the formation stage, which is a clear evidence of the high efficiency of direct-contact heat-transfer processes. In all cases, the bubble reaches the liquid temperature much before half the residence time has elapsed. As observed previously in the transient behaviour of the mean concentration, when heat transfer occurs, the mean bubble temperature transient profile also exhibits a cusp at the moment of detachment, whose existence is also related to the interruption of the gas injection. During the formation stage, the bubble energy loss to the liquid is partially counterbalanced by the energy supplied by gas injection, which smooths the drop in the bubble mean temperature. After detachment, since no more gas is injected into the bubble, this partial counterbalance is eliminated, and the rate of mean temperature decrease grows accordingly.

The most straightforward explanation for the changes in the concentration profiles observed in Fig. 8(a) would be variations in the overall mass-transfer coefficient brought about, for instance, by an increase in the aroma diffusion coefficient with temperature. However, as shown in Fig. 8(b), regardless of the gas inlet temperature, the mean bubble temperature is already quite close to the liquid one for values of $\tau$ as low as 0.3, while the differences in the concentration profile are still significant up to $\tau$ values of about 0.7. Actually, as evidenced by the $K$ values plotted in Fig. 9 (a) as a function of the dimensionless time for the different gas inlet temperatures, the changes in the overall mass-transfer coefficient with the gas inlet temperature are not much significant and, more importantly, they bear little resemblance to the differences in the concentration profiles. In fact, in order to elucidate the behaviour observed in Fig. 9(a), a new aspect has to be taken into account, namely, the bubble volume variations due to the gas density changes which accompany the temperature variations. This aspect is made clear in Fig. 9(b), which portrays the transient evolution of the bubble radius for the four gas inlet temperatures considered in this work.

For a constant mass injection flow rate of gas, which corresponds to the case adopted in this work, an increase in the inlet temperature results in a higher volumetric injection flow rate, and, as a result, the bubble must grow faster, which is precisely the pattern verified in the first part of Fig. 9(b). With a greater rate of growth, the bubble reaches the detachment condition earlier. However, due to bubble contraction caused by heat loss, the bubble volume at the end of the formation stage varies very little, which is in agreement with the findings of Campos and Lage [43]. These facts are all quantitatively displayed in Table 3. According to the data in Fig. 8(b), for hot gas injection, the mean bubble temperature at the end of the formation stage is always greater than the liquid one. Therefore, as the bubble ascends, heat transfer takes place, the bubble mean temperature falls, and, on account of the resulting increase in the gas density, the bubble radius decreases, up to the point at which the liquid and gas temperatures become equal. The higher the gas temperature at the detachment, the larger the extent of this

Table 3
Effect of gas temperature on the simulated results for air stripping of a diluted ethyl acetate solution

| $T_I$ (K) | $G_I$ (mm$^3$/s) | $t_f$ (ms) | $t_{res}$ (s) | $R_{b,f}$ (mm) | $\bar{R}_{f,res}$ (mm) | $\bar{k}_G^2$ (cm/s) | |
|---|---|---|---|---|---|---|---|
| | | | | | | Formation | Ascension |
| 298 | 0.3854 | 79.1 | 0.369 | 1.940 | 1.941 | 2.17 | 1.65 |
| 373 | 0.4823 | 74.8 | 0.372 | 1.937 | 1.907 | 2.14 | 1.68 |
| 473 | 0.6116 | 70.5 | 0.367 | 1.935 | 1.871 | 2.10 | 1.70 |
| 573 | 0.7408 | 67.1 | 0.365 | 1.934 | 1.841 | 2.07 | 1.73 |

effect. This reasoning is made clearer by means of a comparison between the data in Figs. 8(b) and 9(b), which evidences that the bubble radius and bubble mean temperature decreases occur within the same time interval during the ascension stage. With the reduction in the bubble radius, the augmentation of the gas inlet temperature shortens the diffusive path, favouring mass transfer to the bubble, which is the main reason for the pattern verified in Fig. 8(a) during the ascension stage. The increase in the diffusion coefficient does also contribute to it, but only in the short time interval at which heat transfer still takes place.

Also listed in Table 3 are the time-averaged $k_G$ values ($\bar{k}_G^2$) calculated for each gas inlet temperature considered. For the formation stage, a slight reduction in mean value of the gas-side mass-transfer coefficient is observed as the gas inlet temperature rises. Although true that, at the very beginning of the formation stage, higher volumetric flow rates ensure larger $k_G$ values due to enhancement of the radial velocity inside the bubble, this effect is quickly reduced due to the high heat-transfer efficiency. As seen in Fig 8(b), almost immediately after the start of bubble growth, the maximum difference between mean bubble temperatures is already reduced to about 75 K. With regard to the ascension stage, the mean $k_G$ value increases when the gas inlet temperature is raised, even though the effect is still small, for an almost two-fold variation in the gas temperature brings about only a 5% increment in $k_G$. This effect is a consequence of the reduction in the diffusive length. Indeed, the relative differences between mean bubble radius $\bar{R}_{b,res}$ for two gas inlet temperatures are rather consistent with the ones associated with the corresponding mean gas-side mass-transfer coefficients.

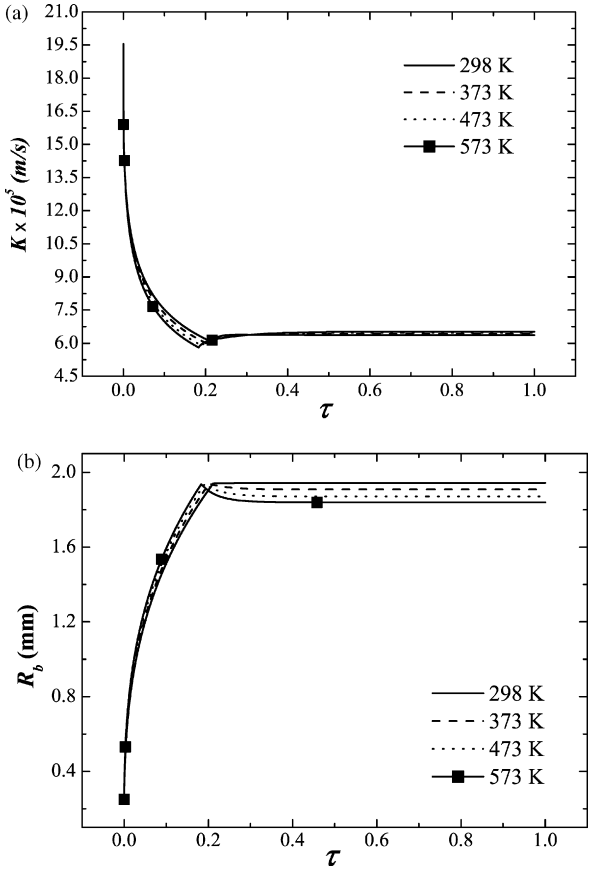


Fig. 9. Transient evolution of the overall mass-transfer coefficient (a) and the bubble radius (b) during the stripping of a dilute ethyl acetate solution with different gas inlet temperatures.

## 5. Conclusions

Gas-side mass-transfer coefficients for the air-stripping of an aroma compound, namely, ethyl acetate, were calculated by means of a recently developed and experimentally validated model for the simultaneous heat and multicomponent mass transfer during the formation and ascension of bubbles.

For isothermal and non-isothermal bubbling, the formation stage was associated with a sheer drop in the $k_G$ value, whose variation covered more than three orders of magnitude and was related to changes in the radial velocity during gas injection. For the ascension stage, in contrast, an almost constant $k_G$ was verified.

For the stripping example analysed, the importance of the gas-side resistance in the process was clearly evidenced. It can not be neglected in any of the analysed cases and it was usually the dominant resistance to mass transfer.

The use of time-averaged $k_G$ values together with a much simpler model for the mass-transfer process was shown to give sufficiently accurate predictions of the final mean ester concentration in the bubble for both the formation and ascension stages, with relative deviations lower than 6%. In particular, for the ascension stage, even the transient behaviour could be well described using the time-averaged $k_G$ for all cases. This result shows that the decomposition of a mass-transfer bubbling process into bubble formation and ascension stages with different constant $k_G$ values, as suggested by [18,32], is indeed sound. Moreover, the detailed model can be used for the prediction of these mean constant $k_G$ values that can be used in more advanced models for gas stripping in bubble columns, such as an Eulerian–Eulerian CFD simulation [25].

In the case of non-isothermal stripping, mean $k_G$ values showed little dependence upon the gas inlet temperature for the formation stage in the range studied. For the ascension stage, a 5% increase in the time-averaged $k_G$ value was observed when the gas inlet temperature was raised from 298 to 573 K.

## Acknowledgements

The authors would like to thank CNPq (grant no. 301548/2005-6) and FAPERJ (E-26/150.397/2004) for the financial support provided.

## References

[1] C.P. Ribeiro Jr., P.L.C. Lage, Gas–liquid direct-contact evaporation: a review, Chem. Eng. Technol. (2005) 1081–1107.
[2] Y.T. Shah, B.G. Kelkar, S.P. Godbole, W.-D. Deckwer, Design parameters estimations for bubble column reactors, AIChE J. 28 (1982) 353–379.
[3] J.J. Heijnen, K. Van't Riet, Mass-transfer, mixing and heat-transfer phenomena in low viscosity bubble column reactors, Chem. Eng. J. 28 (1984) B21–B-42.
[4] W.-D. Deckwer, A. Schumpe, Improved tools for bubble column reactor design and scale-up, Chem. Eng. Sci. 48 (1993) 889–911.
[5] P.H. Calderbank, M.B. Moo-Young, The continuous phase heat and mass transfer properties of dispersions, Chem. Eng. Sci. 16 (1961) 39–54.
[6] G.A. Hughmark, Holdup and mass transfer in bubble columns, Ind. Eng. Chem. Process Des. Dev. 6 (1967) 218–220.
[7] K. Akita, F. Yoshida, Bubble size, interfacial area and liquid-phase mass-transfer coefficients in bubble columns, Ind. Eng. Chem. Process Des. Dev. 13 (1974) 84–91.
[8] M. Nakanoh, F. Yoshida, Gas absorption by Newtonian and non-Newtonian liquids in a bubble column, Ind. Eng. Chem. Process Des. Dev. 19 (1980) 190–195.
[9] H. Hikita, S. Asai, K. Tanigawa, K. Segawa, M. Kitao, The volumetric liquid-phase mass-transfer coefficient in bubble columns, Chem. Eng. J. 22 (1981) 61–67.
[10] E. Shpirt, Role of hydrodynamic factors in ammonia desorption by diffused aeration, Water Res. 15 (1981) 739–743.
[11] S.S. Öztürk, A. Schumpe, W.-D. Deckwer, Organic liquids in a bubble column: holdups and mass-transfer coefficients, AIChE J. 33 (1987) 1473–1480.
[12] P.M. Wilkinson, H. Haringa, L.L.V. Dierendonck, Mass transfer and bubble size in a bubble column under pressure, Chem. Eng. Sci. 49 (1994) 1417–1427.
[13] A. Behkish, Z. Men, J.R. Inga, B.I. Morsi, Mass transfer characteristics in a large-scale slurry bubble column reactor with organic liquid mixtures, Chem. Eng. Sci. 57 (2002) 3307–3324.
[14] Y. Kawase, B. Halard, M. Moo-Young, Theoretical prediction of volumetric mass-transfer coefficients in bubble columns for Newtonian and non-Newtonian fluids, Chem. Eng. Sci. 42 (7) (1987) 1609–1617.
[15] A.D. Polyanin, A.V. Vyaz'min, Mass and heat transfer between a drop or bubble and a flow, Theor. Found. Chem. Eng. 29 (1995) 229–240.
[16] S.S. Ponoth, J.B. McLaughlin, Numerical simulation of mass transfer for bubbles in water, Chem. Eng. Sci. 55 (2000) 1237–1255.
[17] D.S. Walia, D. Vir, Interphase mass transfer during drop or bubble formation, Chem. Eng. Sci. 31 (1976) 525–533.
[18] F.A.N. Rocha, J.R.F. Guedes de Carvalho, Absorption during gas injection through a submerged nozzle. Part I. Gas-side and liquid-side transfer coefficients, Chem. Eng. Res. Des. 62 (1984) 303–320.
[19] M.N.C. Pinheiro, Liquid-phase mass-transfer coefficients for bubbles growing in a pressure field: a simplified analysis, Int. Commun. Heat Mass Transfer 27 (2000) 99–108.
[20] J. Patoczka, D.J. Wilson, Kinetics of the desorption of ammonia from water by diffused aeration, Sep. Sci. Technol. 19 (1984) 77–93.
[21] T. Lionel, D.J. Wilson, D.E. Pearson, Removal of refractory organics from water by aeration. I. Methyl chloroform, Sep. Sci. Technol. 16 (1981) 907–935.
[22] B. Harkins, T.L. Boehm, D.J. Wilson, Removal of refractory organics by aeration. VIII. Air stripping of benzene derivatives, Sep. Sci. Technol. 23 (1988) 91–104.
[23] C. Velázquez, L.A. Estévez, Stripping of trihalomethanes from drinking water in a bubble-column aerator, AIChE J. 38 (1992) 211–218.
[24] C.P. Ribeiro Jr., C.P. Borges, P.L.C. Lage, A combined gas-stripping vapour permeation process for aroma recovery, J. Membr. Sci. 238 (2004) 9–19.
[25] R.C. Rodrigues, Scale-up study of volatile compounds stripping with the aid of computational fluid dynamics, MSc Thesis, Rio de Janeiro, PEQ, COPPE/UFRJ, 2005, 110 p. (in Portuguese).
[26] M.N.C. Pinheiro, J.R.F. Guedes de Carvalho, Stripping in a bubbling pool under vacuum, Chem. Eng. Sci. 49 (1994) 2689–2698.
[27] J.S. Smith, K.T. Valsaraj, Bubble column reactors for wastewater treatment. 3. Pilot-scale solvent sublation of pyrene and pentachlorophenol from simulated wastewater, Ind. Eng. Chem. Res. 36 (1997) 903–914.
[28] N. Nirmalakhandan, W. Jang, W.R.E. Speece, Removal of 1,2-dibromo-3-chloropropane by countercurrent cascade air stripping, J. Environ. Eng. 118 (1992) 226–237.
[29] V.D. Mehta, M.M. Sharma, Effect of diffusivity on gas-side mass-transfer coefficient, Chem. Eng. Sci. 21 (1966) 361–365.
[30] M. Filla, J.F. Davidson, J.F. Bates, M.A. Eccles, Gas phase controlled mass transfer from a bubble, Chem. Eng. Sci. 31 (1976) 359–367.
[31] J.S. Cho, N. Wakao, Determination of liquid-side and gas-side volumetric mass-transfer coefficients in a bubble column, J. Chem. Eng. Jpn. 21 (1988) 576–581.
[32] J.R.F. Guedes de Carvalho, F.A.N. Rocha, M.I. Vasconcelos, M.C.M. Silva, F.A.R. Oliveira, Mass transfer during bubbling in single and multi-orifice absorbers, Chem. Eng. Sci. 41 (19861987–1994).
[33] C.P. Ribeiro Jr., C.P. Borges, P.L.C. Lage, Modelling of direct-contact evaporation using a simultaneous heat and multicomponent mass transfer model for superheated bubbles, Chem. Eng. Sci. 60 (2005) 1761–1772.
[34] W.K. Lewis, W.G. Whitman, Principles of gas absorption, Ind. Eng. Chem. 16 (1924) 1215–1220.
[35] R.E. Treybal, Mass-transfer Operations, 3rd ed., McGraw-Hill, Singapore, 1981, p. 784.
[36] R. Kumar, N.R. Kuloor, The formation of bubbles and drops, Adv. Chem. Eng. 8 (1970) 255–368.
[37] J.F. Davidson, B.O.G. Schuler, Bubble formation at an orifice in a viscous liquid, Trans. Inst. Chem. Eng. 38 (1960) 144–154.
[38] L.R. Petzold, DASSL Code, Version 1989. L316, Computing and Mathematics Research Division, Lawrence Livermore National Laboratory, Livermore.
[39] T.E. Daubert, R.P. Danner, Data compilation tables of properties of pure compounds, Am. Inst. Chem. Eng. (1985).
[40] P.L.C. Lage, Vaporisation of multicomponent droplets in convective and radiant fields, DSc Thesis, Rio de Janeiro, PEQ, COPPE/UFRJ, 1992, 232 p.
[41] R.C. Reid, J.M. Praunsnitz, B.E. Poling, The Properties of Gases and Liquids, 4th ed., McGraw-Hill, New York, 1987, p. 741.
[42] M.F. Sancho, M.A. Rao, D.L. Downing, Infinite dilution activity coefficients of apple juice aroma compounds, J. Food Eng. 34 (1997) 145–158.
[43] F.B. Campos, P.L.C. Lage, Heat and mass transfer modelling during the formation and ascension of superheated bubbles, Int. J. Heat Mass Transf. 43 (2000) 2883–2894.